ACS OMEGA

http://pubs.acs.org/journal/acsodf

Article

Peering into the Formation of Template-Free Hierarchical Flowerlike Nanostructures of $SrTiO_3$

Anderson Thesing, Eduardo J. Damiani, Lara F. Loguercio, Pedro G. Demingos, André R. Muniz, Neftali L. V. Carreño, Sherdil Khan, Marcos J. L. Santos, Alexandre G. Brolo,* and Jacqueline F. L. Santos*

Cite This: *ACS Omega* 2020, 5, 33007−33016

Read Online

ACCESS | Metrics & More | Article Recommendations | Supporting Information

ABSTRACT: The development of efficient advanced functional materials is highly dependent on properties such as morphology, crystallinity, and surface functionality. In this work, hierarchical flowerlike nanostructures of $SrTiO_3$ have been synthesized by a simple template-free solvothermal method involving poly(vinylpyrrolidone) (PVP). Molecular dynamics simulations supported by structural characterization have shown that PVP preferentially adsorbs on {110} facets, thereby promoting the {100} facet growth. This interaction results in the formation of hierarchical flowerlike nanostructures with assembled nanosheets. The petal morphology is strongly dependent on the presence of PVP, and the piling up of nanosheets, leading to nanocubes, is observed when PVP is removed at high temperatures. This work contributes to a better understanding of how to control the morphological properties of $SrTiO_3$, which is fundamental to the synthesis of perovskite-type materials with tailored properties.

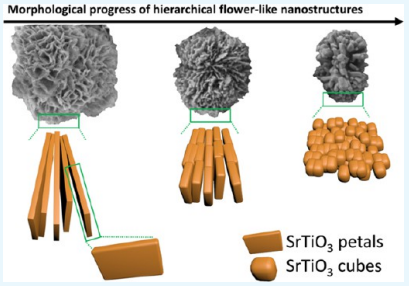

INTRODUCTION

According to Landolt−Boernstein,[1] the generic structure of perovskite-type oxides ABO_3 can accommodate 30 different elements on the A site and half of the periodic table on the B site. This versatility in terms of structure and chemical composition is hardly found in any other class of materials and provides an exceptional opportunity to tailored properties and functionalities for different applications.[2−7] Among the ABO_3 perovskites, strontium titanate ($SrTiO_3$) exhibits an ideal cubic perovskite-type structure with the space group Pm3m in a corner-sharing network of BO_6 octahedral in a wide range of temperature ranging from −160 to 2080 °C, providing a high thermodynamic stability.[8] In addition, it has been reported to be an important n-type semiconductor widely used in different applications, such as photocatalysts for water splitting, electron-transport layers in perovskite solar cells, gas sensors, energy storage devices, and multitasking cost-effective catalysts for condensation, hydrogenation, and amination reactions.[5,7,9−11]

Solvothermal synthesis is certainly one of the most interesting and simple ways to easily obtain $SrTiO_3$ nanostructures with a controlled morphology, crystallinity, chemical composition, and size. The solvothermal approach allows the synthesis to be carried out in a wide range of temperatures (40−250 °C) and using different soluble strontium precursors, such as nitrates, chlorates, acetates, and hydroxides.[12−15] In addition, the use of titanium precursors, such as butoxides, isopropoxides, and chlorides, in solvothermal processes allows a certain degree of control over the rate of hydrolysis by the modulation of nucleation and growth rates, resulting in a drastic selection of morphologies.[16,17] In most of the materials, the growth rate of a crystal is kinetically controlled, as specific facets grow faster to decrease the total surface free energy of the particle. Hence, a lot of efforts have been devoted to the understanding and control of the facets;[18−21] for instance, the predominant formation of desirable surfaces was achieved by adjusting the synthetic route.[22−24] Several efforts have been made to synthesize different $SrTiO_3$ morphologies.[12,25] In particular, $SrTiO_3$ hierarchical nanostructures are potential candidates for energy applications with improved performances relative to their counterparts.[26] Previously, such structures have been synthesized through template-assisted methods,[27−29] which involve complex steps and are not cost effective. On the other hand, a few attempts of template-free synthesis have been described in the literature.[30−32] In any case, there is still plenty of room for the development of simple methodologies to obtain hierarchical nanostructured perovskite nanomaterials.

Surface chemistry plays a crucial role in tuning the properties of solid-state materials, mainly in the nanoscale regime with large surface-to-volume ratios.[33] The (100) plane

Received: September 5, 2020
Accepted: December 3, 2020
Published: December 16, 2020

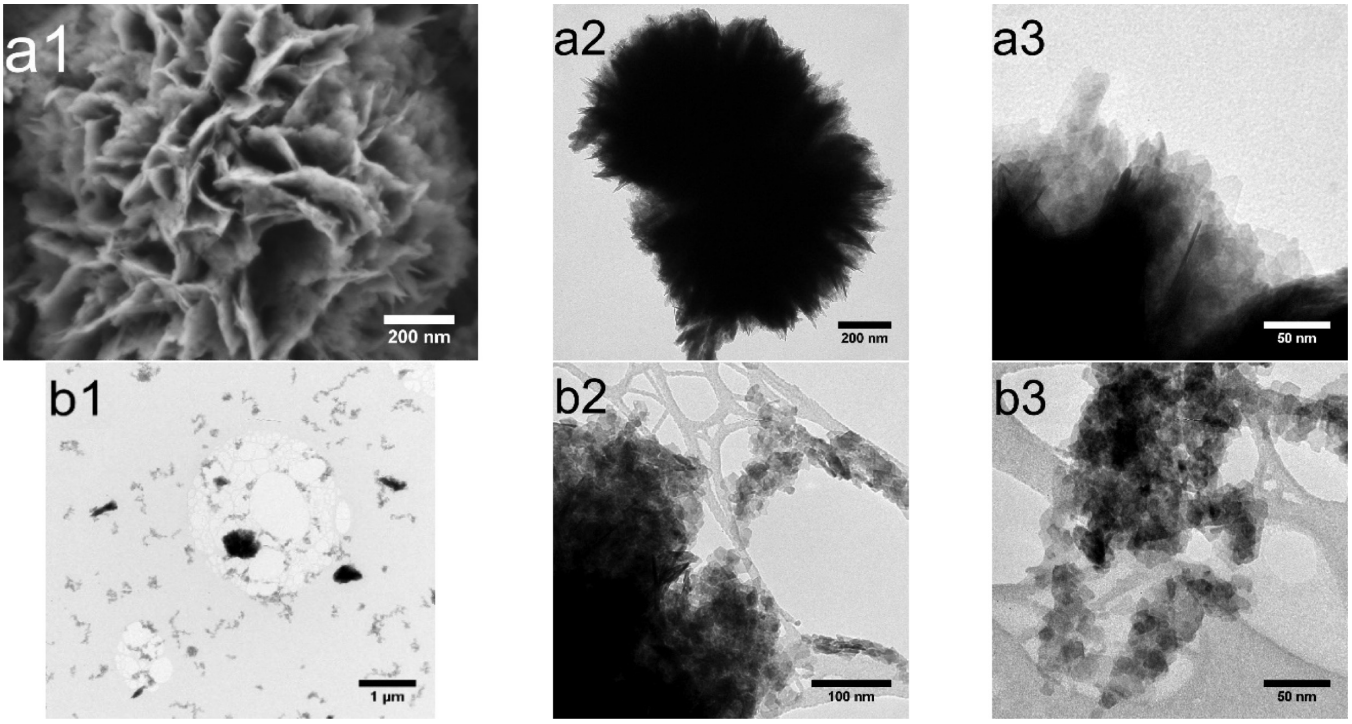

Figure 1. (a) SEM (a1) and TEM (a2−a3) images of the as-synthesized samples obtained after the solvothermal reaction for 12 h in the presence of PVP. (b) TEM images (b1−b3) of the as-synthesized samples obtained under the same conditions as those in (a) but without PVP.

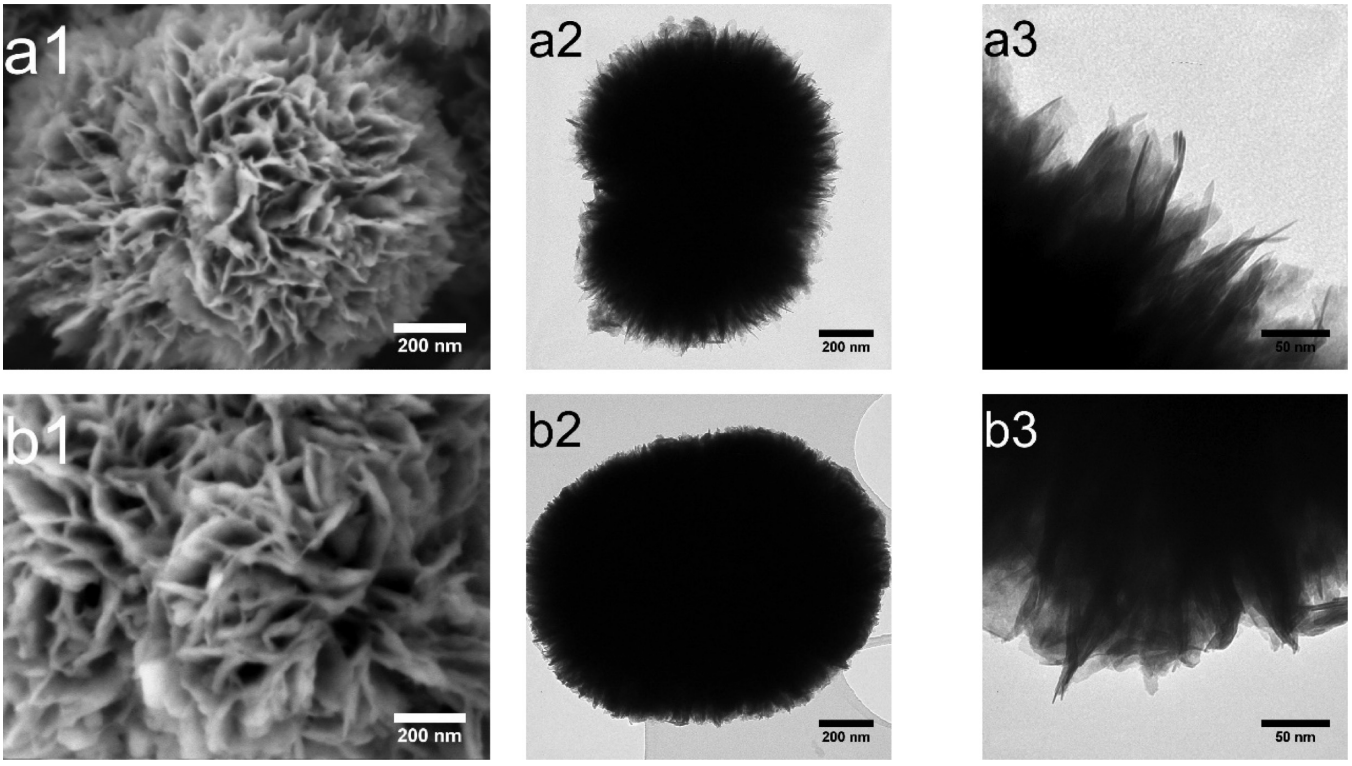

Figure 2. SEM (1) and TEM (2, 3) images of $SrTiO_3$ samples after the solvothermal reaction of (a) 6 h and (b) 3 h.

presents the lowest surface energy in $SrTiO_3$; hence, the most suitable and stable morphology of a particle is a cube bounded by the (100) facets.[34−36] Facet control during synthesis is then required to drive noncubic morphologies. As an example, Xu et al. used the solvothermal method and ethylene glycol (EG), which adsorbs onto (110) facets, to produce $SrTiO_3$ nanosheets; however, a complete formation of regular hierarchical nanostructures was not achieved.[37] Previous studies have shown that poly(vinylpyrrolidone) (PVP) can easily bind to metal oxide surfaces[38−40] to affect surface energy and influence crystal nucleation and growth. The Yang group used PVP with templating microspheres of TiO_2 to obtain

https://dx.doi.org/10.1021/acsomega.0c04343
ACS Omega 2020, 5, 33007−33016

litchilike $SrTiO_3$ structures in a hydrothermal setup.[41] After synthesizing $SrTiO_3$ by the solvothermal method, Zhao et al. produced an $SrTiO_3$−PVP thin film in which PVP acted as trapping centers for memory devices. The observed strong interaction between PVP and $SrTiO_3$ in thin films allowed promising results in device performance.[42]

In this work, the hierarchical nanostructures of $SrTiO_3$ were synthesized using PVP in a template-free solvothermal process. The morphological, structural, and crystalline control of $SrTiO_3$ hierarchical nanostructures is presented. The PVP interactions with different $SrTiO_3$ facets were investigated experimentally, and the findings were supported through molecular dynamics simulations. The conversion of the resulting petal structures from nanosheets to nanocubes by thermal treatment while preserving the hierarchical morphology was demonstrated. The mechanism of morphological and crystal growth was comprehensively elucidated by a variety of characterization techniques.

RESULTS AND DISCUSSION

Figure 1 compares the morphology of the as-prepared samples with and without PVP during a 12 h solvothermal synthesis. The presence of PVP (Figure 1a1−a3) has a tremendous effect on the morphology. Clearly, a hierarchical flowerlike morphology surrounded by nanosheets, named here as "petals," is obtained with PVP; otherwise, nanosheets-like structures are observed in the absence of PVP (Figure 1b1−b3). The morphology obtained in the PVP-free synthesis corroborates previous reports.[37,43] The average size of the flowerlike structures was 1.1 ± 0.2 μm, and the average thickness of the petals was ca. 15.3 ± 5.1 nm. On the other hand, the nanostructures observed in the PVP-free synthesis were ca. 13.8 ± 4.1 nm in size.

The results in Figure 1 strongly suggest that PVP is key to the production of a hierarchical flowerlike morphology, even in the absence of templates.[27−29] The synthesis can be made more cost effective by decreasing the solvothermal reaction time. Figure 2 displays the SEM and TEM images of the as-prepared samples after 6 and 3 h of the solvothermal reaction. The morphology observed in Figure 2 does not differ much from Figure 1a1−a3. The average size and petal thickness of the samples shown in Figure 1a1−a3 and Figure 2 highlight that the morphology is not reaction time dependent. The XRD patterns of the as-synthesized samples were acquired as a function of reaction time (Figure S1), once it may have affected the crystal structure.[44] $SrTiO_3$ (JCPDS No. 35-0734) and $SrCO_3$ (JCPDS No. 05-0418) related to unreacted $Sr(OH)_2$ are observed. One can observe that the amount of $SrTiO_3$ increased with reaction time relative to the amount of $SrCO_3$. Therefore, reaction time shorter than 3 h was not attempted in this study, and we have chosen the sample prepared in the 3 h solvothermal reaction for further characterization.

Molecular dynamics simulations were carried out to elucidate the formation of hierarchical flowerlike nanostructures in the presence of PVP. The likelihood of PVP adsorption on either the {100} or the {110} facets of the flowerlike nanostructures was compared. PVP oligomers were placed in contact with different $SrTiO_3$ surfaces in equilibrium at 160 °C, as described in the Experimental Section. Figure 3 presents the PMF profiles computed to assess the relative affinity of PVP with the different surfaces. A higher adsorption energy (ΔE_{ads}) was found for the {110} (−9.5 kJ.mol^{-1}) and

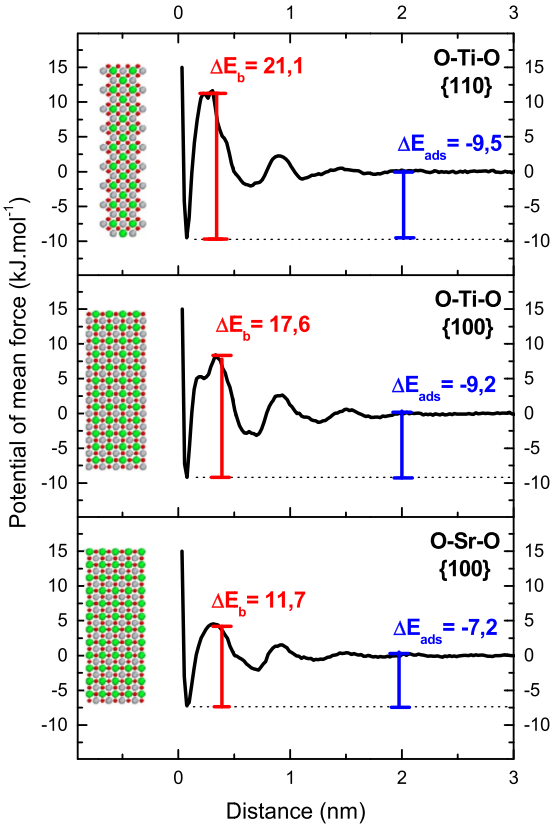

Figure 3. PMF computed from molecular dynamics simulations of the interfacial interaction of vinylpyrrolidone trimers on $SrTiO_3$ facets. Inset: structure of surface crystal terminations (green: Sr^{2+}; gray: Ti^{4+}; and red: O^{2-}).

{100} (−9.2 kJ.mol^{-1}) facets for TiO_2-terminated surfaces when compared to the {100} facet in contact with the SrO-terminated surface (−7.2 kJ·mol^{-1}) (Figure 3). The energy difference is justified by the lower partial charge of strontium ions on the {100} SrO surface compared to titanium, which weakens the interaction with the polar groups of the oligomers. However, the differences between the adsorption energies on the {110} and {100} facets of TiO_2 are not significant. Interestingly, Figure 3 shows that the adsorption/desorption activation energy (E_b) is significantly higher for the {110} facet (21.1 kJ.mol^{-1}) in TiO_2 relative to both the {100} facet in TiO_2 (17.6 kJ.mol^{-1}) and the {100} facet in SrO (11.7 kJ.mol^{-1}). These results lead to the conclusion that the adsorbed PVP molecules are more labile on the {100} surfaces than on the {110} facets, stabilizing the latter from a kinetic point of view. This effect might favor the crystal growth along the {100} facets, which is, in fact, the lowest surface energy facet in $SrTiO_3$.[45] This assumption is strongly supported by the XRD patterns of the samples obtained after the solvothermal reaction for 12 h in the presence and absence of PVP (Figure S6), where the ratio $I_{(110)}/I_{(100)}$ was found to increase from 3.3 to 6.7, respectively. Therefore, during the solvothermal process, PVP strongly adsorbs onto the {110} facet and acts as a self-assembly nucleation guide for the formation of hierarchical flowerlike structures.

The as-prepared samples were heat treated at 300, 400, 500, 750, and 1000 °C. In addition to show that the $SrTiO_3$ (JCPDS No. 35-0734) peaks turn sharper and intense as the temperature was increased from 300 to 1000 °C, Figure 4

https://dx.doi.org/10.1021/acsomega.0c04343
ACS Omega 2020, 5, 33007−33016

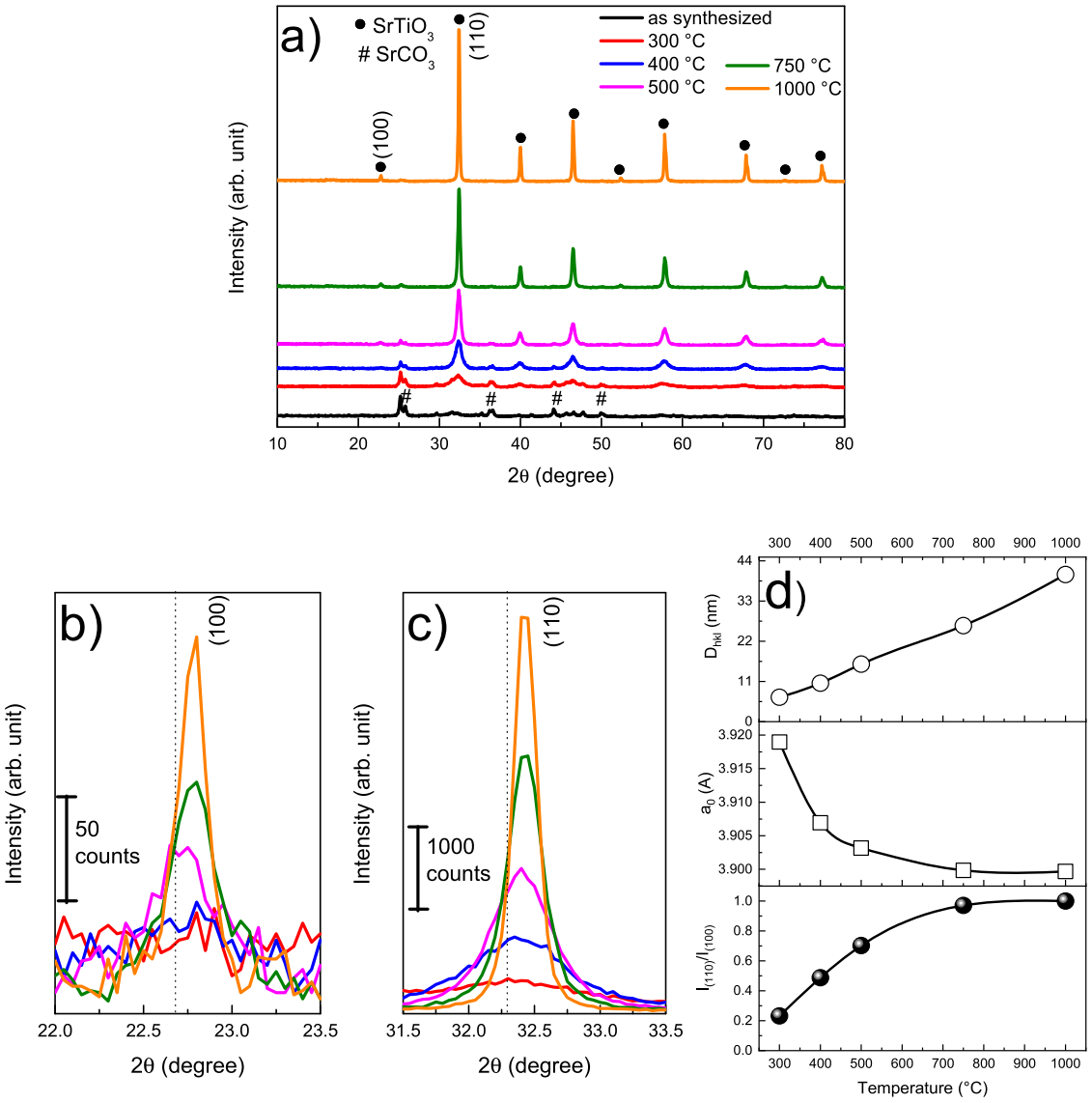

Figure 4. (a) XRD patterns of $SrTiO_3$ hierarchical nanostructures after thermal treatment from 300 to 1000 °C; (b) enlarged version of the regions containing the (100) and (c) the (110) characteristic peaks; and (d) D_{hkl}, a_0 cell parameters, and intensity ratios as a function of the post-heat treatment.

indicates a decrease in the $SrCO_3$ at temperatures higher than 500 °C. The reason for $SrCO_3$ phase depletion with increasing temperature is still unclear. We believe that the $SrCO_3$ reacts directly with the titanium species to yield the $SrTiO_3$ phase, as observed before.[46] The intensity ratios of the (110) characteristic peak to the (100) peak, i.e., $I_{(110)}/I_{(100)}$, presented an exceptional temperature dependency, as indicated in Figure 4d. This ratio increases up to 750 °C and becomes nearly invariant for higher temperatures, strongly suggesting a favored growth of the {110} facets (Figure 4d). The lattice parameter (a_0) and the crystallite size (D_{hkl}) were calculated using Bragg's law and the Scherrer equation (see the Supplementary Information) from the highest intensity peak, i.e., (110) direction and are also displayed in Figure 4d. The lattice parameter a_0 decreased up to 750 °C, resulting in the unit cell volume contraction; hence, a crystal structure with shorter bond lengths is formed. On the other hand, the calculated a_0 at 750 °C (a_0 = 3.8998 Å) and higher temperatures is closer to the ideal cubic structure (a_0 = 3.9050 Å, from JCPDS No. 350734).

Figure 4d shows that the average crystallite size increases linearly from 6 to 40 nm. These results indicate that the post-heat treatment has a profound effect on the overall crystal growth, which leads to morphological changes. The SEM and TEM images of the thermally treated samples are compared in Figure 5, and the morphological parameter distributions are displayed in Figure S2. Nearly no change in the size and morphology is observed in Figure 5 for 300 and 400 °C; however, significant changes started to be observed at 500 °C. The average size of the flowerlike nanostructure decreased from ca. 1.15 ± 0.2 μm at 300 °C to ca. 0.78 ± 0.1 μm at 1000 °C. The hierarchical structure was preserved at even higher temperatures, but the petal format changed from the lamellar nanosheets to nanocubes. As seen in Figure 5, these nanocubes are thicker and denser compared to the samples thermally treated below 500 °C. These results clearly corroborate the XRD analyses in Figure 4d that presented a decrease in the lattice parameter a_0 to a value close to an ideal cubic structure at a higher temperature (Figure 4d). The same general behavior was observed for samples prepared using either 6 or

https://dx.doi.org/10.1021/acsomega.0c04343
ACS Omega 2020, 5, 33007−33016

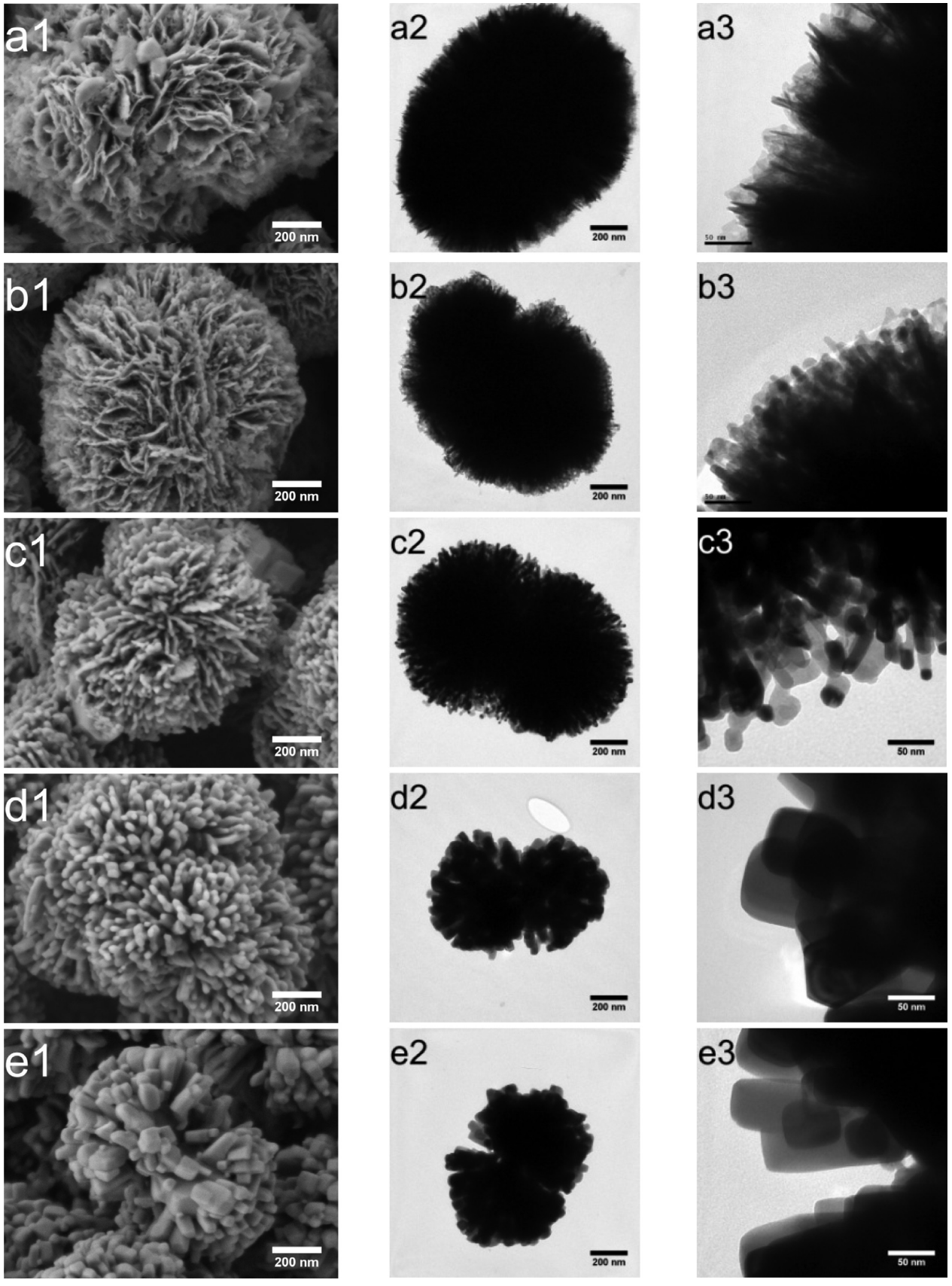

Figure 5. SEM (1) and TEM (2, 3) images of $SrTiO_3$ hierarchical flowerlike nanostructures after thermal treatment at (a) 300, (b) 400, (c) 500, (d) 750, and (e) 1000 °C.

https://dx.doi.org/10.1021/acsomega.0c04343
ACS Omega 2020, 5, 33007−33016

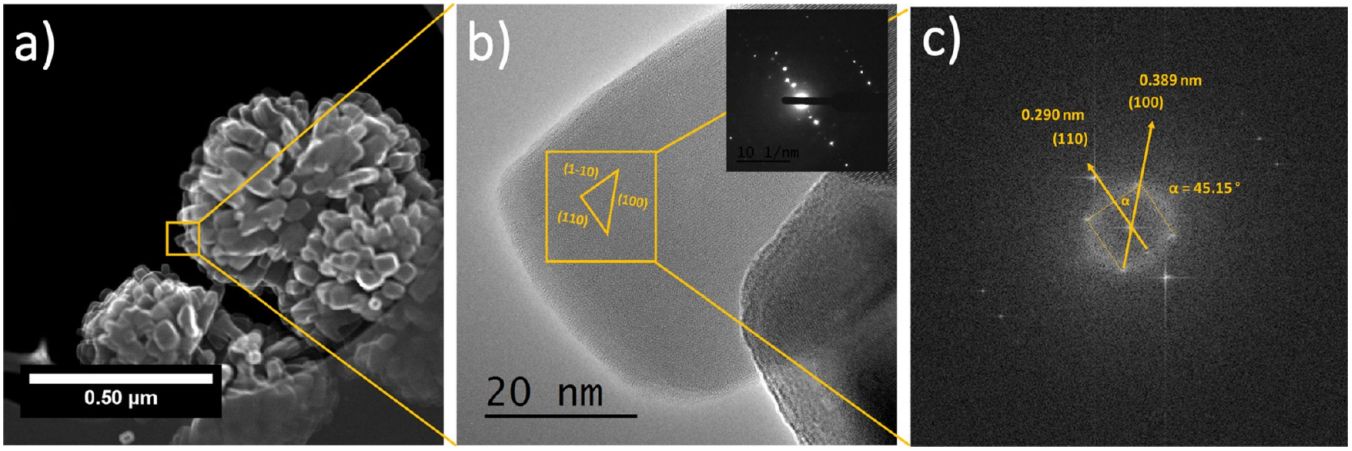

Figure 6. (a) STEM (a secondary electron image), (b) HRTEM image, and (c) FFT of the HRTEM image of the $SrTiO_3$ hierarchical flowerlike nanostructure after thermal treatment of 1000 °C. Inset of (b): selected area electron diffraction pattern.

12 h of solvothermal reaction and subjected to post-heat treatment (see Figures S3 and S4), indicating that the initial amount of $SrTiO_3$ relative to $SrCO_3$ does not affect the morphology after post-heat treatment.

Several syntheses of $SrTiO_3$ that led to the formation of conventional nanocubes have been described.[34,47,48] The key to the formation of hierarchical nanostructures and their morphological control in Figure 1 lies in the presence of EG and PVP, which undergo adsorption on metal oxides.[37] PVP drives the self-assembly of $SrTiO_3$ nanocrystalline nanosheets, and they undergo a crystallization process during the solvothermal reaction, leading to the hierarchical nanostructure formation.[37]

The post-heat treatment clearly demonstrates control over the petal morphology, since it is possible to obtain hierarchical flowerlike structures with either lamellar nanosheets or nanocubes. Figure 6 displays the HRTEM image of nanocubic petals prepared after 3 h of solvothermal reaction and 1000 °C post-heat treatment. The interplanar distances of 0.290 and 0.389 nm correspond to the (110) and the (100) crystallographic planes, respectively. The angle between these planes was 45.15°. The selected area electron diffraction pattern of the petal (inset Figure 6b) shows single spots, suggesting that the perovskite-type oxides have grown and self-orientated to assume single-crystal behavior and exhibit a high order of crystallinity. Figure 6 agrees with the XRD analyses in which the largest crystallite size was observed for this sample, and the a_0-value was closer to the ideal cubic structure (Figure 4d).

The effect of post-heat treatment on the chemical composition was investigated by FTIR and Raman spectroscopy. The IR features shown in Figure 7a display the vibration bands at 1084 and 1030 cm^{-1}, related to the C−C−O vibration of surface-adsorbed EG.[49,50] The bands at 1650 and 1460 cm^{-1} are related to the C═O and pyrrolidinyl groups from the PVP chains.[51] A low intensity band can also be observed for all samples at 856 cm^{-1}. This band can be assigned to the CO_3^{-2} vibration of $SrCO_3$.[52] The broad band within 650−545 cm^{-1} is associated with the perovskite structure of the TiO_6 octahedron stretching vibration mode.[16] This band becomes sharper and shifts to a lower wavenumber with an increase in temperature. This is in accordance with the XRD measurements (Figure 4), where higher temperatures result in a lower a_0 value and a larger crystallite size (D_{hkl}). The inset in Figure 7a shows the changes

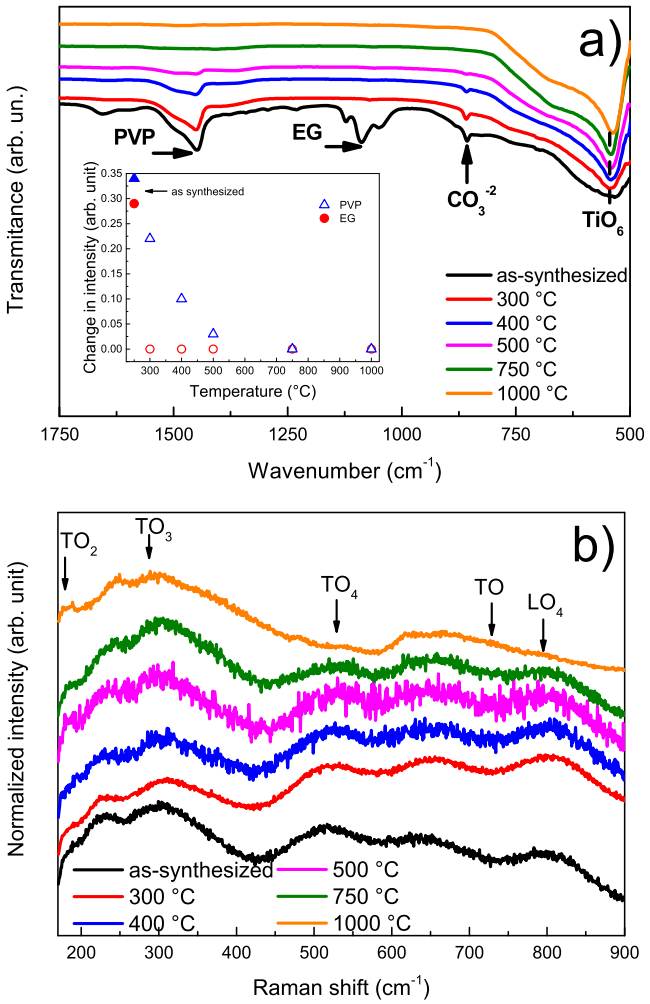

Figure 7. (a) FTIR and (b) Raman spectra of the as-synthetized $SrTiO_3$ hierarchical nanostructures and after thermal treatment from 300 to 1000 °C. The inset in (a) shows the change in the intensity of PVP and EG modes vs post-heat treatment temperature.

in the intensity of PVP (ca. 1460 cm^{-1}) and EG (ca. 1084 cm^{-1}) vibration modes against temperature. EG is not observed for temperatures higher than 300 °C;[49,50] meanwhile, PVP only disappears at temperatures above 500 °C. Interestingly, this is the same temperature where the most

https://dx.doi.org/10.1021/acsomega.0c04343
ACS Omega 2020, 5, 33007−33016

significant change from nanosheets to the cubic morphology was observed (Figure 5).

It is possible to identify a series of first-order scattering broad bands at ca. of 180, 288, 544, 727, and 793 cm^{-1} in the Raman spectra in Figure 7b, corresponding to the TO_2, TO_3, TO_4, TO and LO_4 modes, respectively (Figure 7b).[12,16,53] UV−vis spectroscopy shows no change in the band gap (Figure S5).[2,12,15]

The formation of titanate-based structures was described by a simplified three-stage mechanism.[54,55] In the first stage, the alcohol chains replace the Ti atoms from titanium butoxide, making the hydrolysis of titanium species slower. In the second stage, the hydrolysis leads to the formation of $Ti(OH)_4$ nuclei, which are randomly distributed in the liquid phase. At this point, the strontium ions start to react with titanium species to decrease the formation energy of the final structure. In the third stage, condensation reactions lead to the formation of a network system from the original basic units with stable Ti−O−Ti and Sr−O−Sr bonds, forming $SrTiO_3$ species.[16] Once the nucleation step is completed, like previously observed for EG,[37] we suggest that the PVP also starts to interact with the metal oxide surface. This surface interaction affects the crystal growth, driving the formation of the lamellar nanostructure. After heat treatment, as PVP is removed at temperatures higher than 500 °C, the coarsening and ripening process driven by thermal energy enables the nanosheets to form $SrTiO_3$ nanocubes. Under the experimental conditions explored in this work, this process can explain the temperature-dependent morphological evolution, in which thermodynamically less-stable small particles (nanosheets) transform into large particles (nanocubes) via kinetic pathways, such as surface diffusion. As a result, there is the formation of highly oriented nanocubes.[36,56] PVP-free solvothermal synthesis resulted in the formation of nanosheets (Figure 1), corroborating previous work where the synthesis was performed using only EG.[37,42] Both EG and PVP adsorbed onto $SrTiO_3$ drive the formation of hierarchical flowerlike structures surrounded by nanosheet petals during solvothermal synthesis. Therefore, their integrated presence plays a vital role in the formation of hierarchical nanostructures. Since EG is easily removed during the post-heat treatment (Figure 7a), the results suggest that the most important interaction leading to the preservation of nanosheets in hierarchy is PVP. Once PVP is removed at high temperatures (above 500 °C), a surface reconstruction is initiated to decrease the surface energy, resulting in the more thermodynamically stable cube morphology.[34−36] Crystallographically, the surface interaction of PVP is dominated predominantly with the {110} plane, as confirmed by molecular dynamics simulations. Therefore, the morphology evolves toward a surface energy minimization at high temperatures, guiding the lamellar nanosheets to grow along {100} facets; thereby, the petal structures change from nanosheets into nanocubes. The results suggest that a comprehensive control of the petal morphology can be achieved by tuning the PVP amount in hierarchical nanostructures. A schematic representation of the template-free formation mechanism introduced here is given in Scheme 1.

CONCLUSIONS

The formation of the hierarchical flowerlike $SrTiO_3$ nanostructure is strongly dependent on the presence of EG and PVP during the solvothermal reaction. The organic species interact preferentially with the {110} facets, decreasing the surface energy and inducing the {100} facet growth. The solvothermal reaction time has little effect on the morphology of the hierarchical nanostructures; however, decreasing the reaction time increases the $SrCO_3$ content. Upon high temperature, the morphology evolves toward a surface energy minimization, i.e., structural reorganization densifies the nanoflowers, decreasing their size and transforming the petals into nanocubes. This study has shown a simple, cost-effective, and template-free strategy to achieve a fine control over $SrTiO_3$ morphology and crystallinity. The potential for the fine-tuning morphology of $SrTiO_3$ introduced here can be applied to other perovskite nanostructures that are widely used in energy applications.

Scheme 1. Morphology Evolution through Thermal Treatment

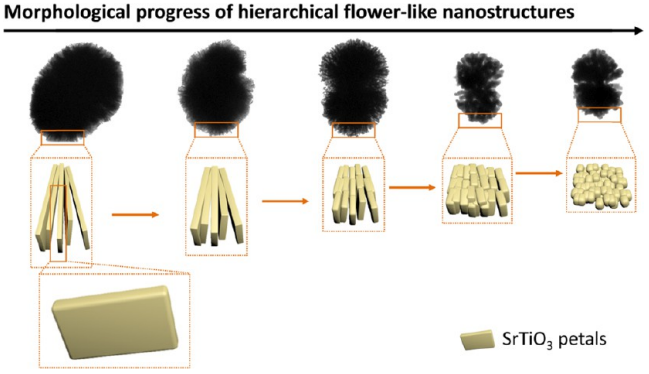

EXPERIMENTAL SECTION

Materials. Titanium butoxide (Sigma-Aldrich, ≥97%), strontium hydroxide octahydrate (Sigma-Aldrich, 95%), ammonium hydroxide (Sigma-Aldrich, 28−30%), ethylene glycol (Química Moderna, 99.5%), poly(vinylpyrrolidone) (Vetec, average mol. wt 40,000), ethanol (Synth, 99.5%), and isopropyl alcohol (Synth, 99.5%) were used as received.

Synthesis of Hierarchical Flowerlike $SrTiO_3$ Nanostructures. Hierarchical flowerlike $SrTiO_3$ nanostructures were synthesized by controlling the hydrolysis of titanium butoxide with EG and PVP. Strontium hydroxide (4.25 g), PVP (0.74 g), ammonium hydroxide (8.0 mL), and EG (40.0 mL) were added to a single-neck glass flask under constant stirring for 30 min. Titanium butoxide (5.44 g) was then added to the solution, and the constant stirring was maintained for another 30 min. After this, the solution was placed in a 170 mL removable Teflon cup in stainless-steel body and heated to 160 °C at a rate of 5 $°C.min^{-1}$ (ventilated electrical heating oven, Marconi) during 12, 6, and 3 h to enable the solvothermal reaction. The samples were rinsed by 5 cycles of centrifugation with ethanol for 5 min each at 2500 rpm.

Heat Treatment − Petal Morphological Control from Nanosheets to Nanocubes. The samples obtained after 3 h of solvothermal synthesis were heat treated for 300, 400, 500, 750, and 1000 °C during 4 h, with a heating and cooling rate of 4 $°C{\cdot}min^{-1}$. The resulting samples were labeled as $SrTiO_3$-*T*, where *T* indicates the temperature of the heat treatment.

Characterization. Transmission electron microscopy (TEM) images were obtained on a Jeol JEM 1200 EXII with an acceleration voltage of 80 kV. The selected area electron diffraction (SAED) and high-resolution transmission electron

https://dx.doi.org/10.1021/acsomega.0c04343
ACS Omega 2020, 5, 33007−33016

microscopy (HRTEM) images were obtained with a Hitachi HF-3300 V STEHM, at an acceleration voltage of 300 kV. A dispersion of the samples in isopropyl alcohol was deposited by drop casting onto a carbon-coated copper grid of 200 mesh. Scanning electron microscopy (SEM) images were obtained on a Zeiss Auriga with an acceleration voltage of 2 kV. Particle size distributions were evaluated using ImageJ software from SEM images (Figure S2). X-ray diffraction patterns were obtained on a Siemens D500 diffractometer with a Cu Kα radiation (λ = 1.54 Å, at 40 kV and 17 mA) in the 2 theta range of 10−80°, with an increment of 0.05°. UV−vis spectroscopy was carried out on a Shimadzu UV-2450PC spectrometer using an integrating sphere at the range of 300−800 nm. Infrared spectroscopy was performed on an FTIR-ATR Bruker Alpha-P within 1750−500 cm^{-1}. Raman spectroscopy was performed using a Renishaw Raman confocal microscope, equipped with a 20× microscope objective (Leyca Microsystems) and a 633 nm laser (He−Ne, Melles Griot).

Classical Molecular Dynamics Simulations. Molecular dynamics simulations were carried out in LAMMPS[57] to study the PVP adsorption on two different $SrTiO_3$ surfaces of interest: {110} and {100} with two different terminations, namely, {100} TiO_2 and {100} SrO. The {110} surface had its strontium atoms removed for stabilization, as suggested before.[58] Slabs, of about 45 × 45 $Å^2$ (periodic along the x and y directions) and a thickness along z (perpendicular to the surface) that is enough for the bulk density far from the surface to reach a constant value, were put in contact with vinylpyrrolidone trimers with density corresponding to its bulk under the relevant conditions, at 433 K (synthesis temperature of 160 °C for solvothermal reaction) for 10 ns (long enough for system equilibration), as performed in similar works.[59] The Nosé−Hoover thermostat was used for temperature control. The atomic positions of the crystal were kept fixed during the simulations. Atomic charges and Lennard-Jones parameters for $SrTiO_3$ surfaces were taken from previous works on the adsorption of organic molecules,[58] and the interatomic interactions for PVP molecules were described using the CHARMM General Force Field,[60] with specific parameters for PVP.[61] The PPPM method was used to compute long-range electrostatic interactions. The LAMMPS initialization files were prepared with the aid of the ChemStruct Python package (https://pypi.org/project/chemstruct/). The bulk density for vinylpyrrolidone was previously determined at 1.0 atm for the force field parameters, showing good agreement with experimental values. Atomic positions were saved every 50 ps to compute the density as a function of position $\rho(z)$,[58] by counting carbonyl oxygen atoms on a fine mesh of domain slices along the z axis (perpendicular to the exposed surface). This density was then used to compute potential of mean force (PMF) profiles along z, using eq 1 as in previous works:[58]

$$\mathrm{PMF}(z) = -RT\ln\left(\frac{\rho(z)}{\rho_0}\right) \quad (1)$$

where R is the gas constant, T is the temperature, and ρ_0 is the bulk density (far from the surface). Therefore, the shown PMF is given as energy per mol of repeating unit. PMF profiles are then used to estimate relative adsorption energies ΔE_{ads} (computed as the difference between the PMF of the bulk phase and the PMF at its lowest value, near the surface) and activation energy barriers for adsorption/desorption E_b (computed as the difference between maximum and minimum PMF values along the z direction) for the three investigated surfaces.

■ ASSOCIATED CONTENT

Supporting Information

The Supporting Information is available free of charge at https://pubs.acs.org/doi/10.1021/acsomega.0c04343.

Experimental details; physiochemical characterization of the samples: structural characterization from XRD; size distribution of the particles; SEM and TEM images; and UV−vis absorption spectra (PDF)

■ AUTHOR INFORMATION

Corresponding Authors

Alexandre G. Brolo − *Department of Chemistry and Center for Advanced Materials and Related Technologies, University of Victoria, Victoria, British Columbia V8W 3V6, Canada;* orcid.org/0000-0002-3162-0881; Email: agbrolo@uvic.ca

Jacqueline F. L. Santos − *Instituto de Química, Universidade Federal do Rio Grande do Sul, Porto Alegre, Rio Grande do Sul 91501-970, Brazil;* orcid.org/0000-0003-2764-0684; Email: jacqueline.ferreira@ufrgs.br

Authors

Anderson Thesing − *Centro de Tecnologias Estratégicas do Nordeste, Recife, Pernambuco 50740-545, Brazil;* orcid.org/0000-0002-3655-9936

Eduardo J. Damiani − *Instituto de Química, Universidade Federal do Rio Grande do Sul, Porto Alegre, Rio Grande do Sul 91501-970, Brazil*

Lara F. Loguercio − *Programa de Pós-graduação em Ciência dos Materiais, Universidade Federal do Rio Grande do Sul, Porto Alegre, Rio Grande do Sul 91501-970, Brazil;* orcid.org/0000-0001-6790-2971

Pedro G. Demingos − *Departamento de Engenharia Química, Universidade Federal do Rio Grande do Sul, Porto Alegre, Rio Grande do Sul 90040-040, Brazil;* orcid.org/0000-0002-3700-8335

André R. Muniz − *Departamento de Engenharia Química, Universidade Federal do Rio Grande do Sul, Porto Alegre, Rio Grande do Sul 90040-040, Brazil*

Neftali L. V. Carreño − *Centro de Desenvolvimento Tecnológico, Universidade Federal de Pelotas, Pelotas, Rio Grande do Sul 96010-610, Brazil*

Sherdil Khan − *Instituto de Física, Universidade Federal do Rio Grande do Sul, Porto Alegre, Rio Grande do Sul 91501-970, Brazil*

Marcos J. L. Santos − *Instituto de Química, Universidade Federal do Rio Grande do Sul, Porto Alegre, Rio Grande do Sul 91501-970, Brazil*

Complete contact information is available at: https://pubs.acs.org/10.1021/acsomega.0c04343

Notes

The authors declare no competing financial interest.

■ ACKNOWLEDGMENTS

The authors gratefully acknowledge the CNPq (process 141655/2017-8 and 141492/2016-3 303439/2015-7, 423244/2016-7, 424769/2018-2, 309454/2018-2, and

305875/2019-1) and CAPES (Financial Code 001, CAPES-PDSE process 88881.132060/2016-01 and 88881.135800/2016-01). Electron microscopy facilities were provided by CAMTEC at UVic and CNANO at UFRGS. The authors acknowledge the Centro Nacional de Supercomputacao (CESUP/UFRGS, Brazil) for providing computational resources for the calculations reported in this paper.

REFERENCES

(1) Robertson, J. H. Landolt−Börnstein. Numerical data and functional relationships in science and technology. Group III. Crystal and solid state physics. *Crystal structure data of inorganic compounds*. Part b by Pies, W.; Weiss, A., Springer, Berlin, 1978; *Vol. 7*. 480.

(2) Grabowska, E. Selected Perovskite Oxides: Characterization, Preparation and Photocatalytic Properties-A Review. *Appl. Catal. B-Environ.* **2016**, *186*, 97−126.

(3) Santander-Syro, A. F.; Copie, O.; Kondo, T.; Fortuna, F.; Pailhés, S.; Weht, R.; Qiu, X. G.; Bertran, F.; Nicolaou, A.; Taleb-Ibrahimi, A.; LeFvre, P.; Herranz, G.; Bibes, M.; Reyren, N.; Apertet, Y.; Lecoeur, P.; Barthélémy, A.; Rozenberg, M. J. Two-Dimensional Electron Gas with Universal Subbands at the Surface of SrTiO 3. *Nature* **2011**, *469*, 189−193.

(4) Burnside, S.; Moser, J.-E.; Brooks, K.; Grätzel, M.; Cahen, D. Nanocrystalline Mesoporous Strontium Titanate as Photoelectrode Material for Photosensitized Solar Devices: Increasing Photovoltage through Flatband Potential Engineering. *J. Phys. Chem. B* **2002**, *103*, 9328−9332.

(5) Hara, T.; Ishiguro, T. Oxygen Sensitivity of SrTiO 3 Thin Film Prepared Using Atomic Layer Deposition. *Sensors ctuators B: Chem.* **2009**, *136*, 489−493.

(6) Jin, Y.; Jiang, D.; Li, D.; Xiao, P.; Ma, X.; Chen, M. SrTiO 3 Nanoparticle/SnNb 2 O 6 Nanosheet 0D/2D Heterojunctions with Enhanced Interfacial Charge Separation and Photocatalytic Hydrogen Evolution Activity. *ACS Sustainable Chem. Eng.* **2017**, *5*, 9749−9757.

(7) Hou, C.; Huang, W.; Zhao, W.; Zhang, D.; Yin, Y.; Li, X. Ultrahigh Energy Density in SrTiO3 Film Capacitors. *ACS Appl. Mater. Interfaces* **2017**, *9*, 20484−20490.

(8) Canu, G.; Buscaglia, V. Hydrothermal Synthesis of Strontium Titanate: Thermodynamic Considerations, Morphology Control and Crystallisation Mechanisms. *CrystEngComm* **2017**, *19*, 3867−3891.

(9) Chiang, T. H.; Lyu, H.; Hisatomi, T.; Goto, Y.; Takata, T.; Katayama, M.; Minegishi, T.; Domen, K. Efficient Photocatalytic Water Splitting Using Al-Doped SrTiO3 Coloaded with Molybdenum Oxide and Rhodium-Chromium Oxide. *ACS Catal.* **2018**, *8*, 2782−2788.

(10) Tsvetkov, N.; Moon, B. C.; Lee, J. Y.; Kang, J. K. Controlled Synthesis of Nanocrystalline Nb:SrTiO3 Electron Transport Layers for Robust Interfaces and Stable High Photovoltaic Energy Conversion Efficiency in Perovskite Halide Solar Cells. *ACS Appl. Energy Mater.* **2020**, *3*, 344−351.

(11) Srilakshmi, C.; Saraf, R.; Shivakumara, C. Structural Studies of Multifunctional SrTiO3 Nanocatalyst Synthesized by Microwave and Oxalate Methods: Its Catalytic Application for Condensation, Hydrogenation, and Amination Reactions. *ACS Omega* **2018**, *3*, 10503−10512.

(12) Souza, A. E.; Santos, G. T. A.; Barra, B. C.; MacEdo, W. D.; Teixeira, S. R.; Santos, C. M.; Senos, A. M. O. R.; Amaral, L.; Longo, E. Photoluminescence of SrTiO 3 : Influence of Particle Size and Morphology. *Cryst. Growth Des.* **2012**, *12*, 5671−5679.

(13) Kimijima, T.; Kanie, K.; Nakaya, M.; Muramatsu, A. Solvothermal Synthesis of Shape-Controlled Perovskite $MTiO_3$ (M = Ba, Sr, and Ca) Particles in H_2O/Polyols Mixed Solutions. *Mater. Trans.* **2013**, *55*, 147−153.

(14) Dong, L.; Shi, H.; Cheng, K.; Wang, Q.; Weng, W.; Han, W. Shape-Controlled Growth of SrTiO<inf>3</Inf> Polyhedral Sub-micro/Nanocrystals. *Nano Res.* **2014**, *7*, 1311−1318.

(15) Da Silva, L. F.; M'Peko, J. C.; Andrés, J.; Beltrán, A.; Gracia, L.; Bernardi, M. I. B.; Mesquita, A.; Antonelli, E.; Moreira, M. L.; Mastelaro, V. R. Insight into the Effects of Fe Addition on the Local Structure and Electronic Properties of SrTiO3. *J. Phys. Chem. C* **2014**, *118*, 4930−4940.

(16) Moreira, M. L.; Longo, V. M.; Avansi, W.; Ferrer, M. M.; Andrés, J.; Mastelaro, V. R.; Varela, J. A.; Longo, É. Quantum Mechanics Insight into the Microwave Nucleation of SrTiO 3 Nanospheres. *J. Phys. Chem. C* **2012**, *116*, 24792−24808.

(17) Kalyani, V.; Vasile, B. S.; Ianculescu, A.; Testino, A.; Carino, A.; Buscaglia, M. T.; Buscaglia, V.; Nanni, P. Hydrothermal Synthesis of SrTiO3: Role of Interfaces. *Cryst. Growth Des.* **2015**, *15*, 5712−5725.

(18) Butburee, T.; Kotchasarn, P.; Hirunsit, P.; Sun, Z.; Tang, Q.; Khemthong, P.; Sangkhun, W.; Thongsuwan, W.; Kumnorkaew, P.; Wang, H.; Faungnawakij, K. New Understanding of Crystal Control and Facet Selectivity of Titanium Dioxide Ruling Photocatalytic Performance. *J. Mater. Chem. A* **2019**, *7*, 8156−8166.

(19) Zhang, D.; Li, G.; Yang, X.; Yu, J. C. A Micrometer-Size TiO2 Single-Crystal Photocatalyst with Remarkable 80% Level of Reactive Facets. *Chem. Commun.* **2009**, *29*, 4381−4383.

(20) Shi, R.; Chen, Y. Controlled Formation of Defective Shell on TiO 2 (001) Facets for Enhanced Photocatalytic CO 2 Reduction. *ChemCatChem* **2019**, *11*, 2270−2276.

(21) Liu, G.; Yang, H. G.; Pan, J.; Yang, Y. Q.; Lu, G. Q. M.; Cheng, H. M. Titanium Dioxide Crystals with Tailored Facets. *Chem. Rev.* **2014**, *114*, 9559−9612.

(22) Yang, H. G.; Sun, C. H.; Qiao, S. Z.; Zou, J.; Liu, G.; Smith, S. C.; Cheng, H. M.; Lu, G. Q. Anatase TiO2 Single Crystals with a Large Percentage of Reactive Facets. *Nature* **2008**, *453*, 638−641.

(23) Joo, J.; Chow, B. Y.; Prakash, M.; Boyden, E. S.; Jacobson, J. M. Face-Selective Electrostatic Control of Hydrothermal Zinc Oxide Nanowire Synthesis. *Nat. Mater.* **2011**, *10*, 596−601.

(24) Barnard, A. S.; Curtiss, L. A. Prediction of TiO 2 Nanoparticle Phase and Shape Transitions Controlled by Surface Chemistry. *Nano Lett.* **2005**, *5*, 1261−1266.

(25) Phoon, B. L.; Lai, C. W.; Juan, J. C.; Show, P. L.; Chen, W. H. A Review of Synthesis and Morphology of SrTiO3 for Energy and Other Applications. *Int. J. Energy Res.* **2019**, *43*, 5151−5174.

(26) Lai, X.-Y.; Wang, C.-R.; Jin, Q.; Yu, R.-B.; Wang, D. Synthesis and Photocatalytic Activity of Hierarchical Flower-like SrTiO3 Nanostructure. *Sci. China Mater.* **2015**, *58*, 192−197.

(27) Wu, Z.; Zhang, Y.; Wang, X.; Zou, Z. Ag@SrTiO3 Nanocomposite for Super Photocatalytic Degradation of Organic Dye and Catalytic Reduction of 4-Nitrophenol. *New J. Chem.* **2017**, *41*, 5678−5687.

(28) Ye, M.; Wang, M.; Zheng, D.; Zhang, N.; Lin, C.; Lin, Z. Garden-like Perovskite Superstructures with Enhanced Photocatalytic Activity. *Nanoscale* **2014**, *6*, 3576−3584.

(29) Ruzimuradov, O.; Hasegawa, G.; Kanamori, K.; Nakanishi, K. Preparation of Hierarchically Porous Nanocrystalline CaTiO3, SrTiO3 and BaTiO3 Perovskite Monoliths. *J. Am. Ceram. Soc.* **2011**, *94*, 3335−3339.

(30) Wu, Q. S.; Liu, J. W.; Chen, S. F.; Liang, H. W.; Yu, S. H. Surfactant-Free Synthesis of SrTiO3 Hierarchical Structures in Ethanol/Water Mixed Solvent at Room Temperature. *CrystEngComm* **2014**, *17*, 6895−6900.

(31) Guo, M.; Liu, Q.; Wu, M.; Lv, T.; Jia, L. Novel Reduced Graphene Oxide Wrapped-SrTiO3 Flower-like Nanostructure with Ti−C Bond for Free Noble Metal Decomposition of Formic Acid to Hydrogen. *Chem. Eng. J.* **2018**, *334*, 1886−1896.

(32) Zou, F.; Jiang, Z.; Qin, X.; Zhao, Y.; Jiang, L.; Zhi, J.; Xiao, T.; Edwards, P. P. Template-Free Synthesis of Mesoporous N-Doped SrTiO 3 Perovskite with High Visible-Light-Driven Photocatalytic Activity. *Chem. Commun.* **2012**, *48*, 8514−8516.

(33) Jacobs, K.; Zaziski, D.; Scher, E. C.; Herhold, A. B.; Alivisatos, A. P. Activation Volumes for Solid-Solid Transformations in Nanocrystals. *Science* **2001**, *293*, 1803−1806.

(34) Dang, F.; Mimura, K. I.; Kato, K.; Imai, H.; Wada, S.; Haneda, H.; Kuwabara, M. Growth of Monodispersed SrTiO3 Nanocubes by Thermohydrolysis Method. *CrystEngComm* **2011**, *13*, 3878−3883.

https://dx.doi.org/10.1021/acsomega.0c04343
ACS Omega 2020, 5, 33007−33016

(35) Niu, J.; Yan, P. X.; Seo, W. S.; Koumoto, K. Hydrothermal Synthesis of SrTiO 3 Nanoplates through Epitaxial Self-Assembly of Nanocubes. *J. Nanosci. Nanotechnol.* **2012**, *12*, 2685−2690.
(36) Kuang, Q.; Yang, S. Template Synthesis of Single-Crystal-like Porous SrTiO3 Nanocube Assemblies and Their Enhanced Photocatalytic Hydrogen Evolution. *ACS Appl. Mater. Interfaces* **2013**, *5*, 3683−3690.
(37) Xu, G.; Huang, X.; Zhang, Y.; Deng, S.; Wei, X.; Shen, G.; Han, G. Self-Assembly and Formation Mechanism of Single-Crystal SrTiO3 Nanosheets via Solvothermal Route with Ethylene Glycol as Reaction Medium. *CrystEngComm* **2013**, *15*, 7206−7211.
(38) Liu, S.; Ho, S.; Chen, Y.; So, F. Passivation of Metal Oxide Surfaces for High-Performance Organic and Hybrid Optoelectronic Devices. *Chem. Mater.* **2015**, *27*, 2532−2539.
(39) Pattanaik, M.; Bhaumik, S. K. Adsorption Behaviour of Polyvinyl Pyrrolidone on Oxide Surfaces. *Mater. Lett.* **2000**, *44*, 352−360.
(40) Briffa, S. M.; Nasser, F.; Valsami-Jones, E.; Lynch, I. Uptake and Impacts of Polyvinylpyrrolidone (PVP) Capped Metal Oxide Nanoparticles on Daphnia Magna: Role of Core Composition and Acquired Corona. *Environ. Sci. Nano* **2018**, *5*, 1745−1756.
(41) Zhao, W.; Wang, H.; Liu, N.; Rong, J.; Zhang, Q.; Li, M.; Yang, X. Hydrothermal Synthesis of Litchi-like SrTiO3 with the Help of Ethylene Glycol. *J. Am. Ceram. Soc.* **2019**, *102*, 981−987.
(42) Chen, G.; Zhang, P.; Pan, L.; Qi, L.; Yu, F.; Gao, C. Flexible Nonvolatile Resistive Memory Devices Based on SrTiO3 Nanosheets and Polyvinylpyrrolidone Composites. *J. Mater. Chem. C* **2017**, *5*, 9799−9805.
(43) Kimijima, T.; Kanie, K.; Nakaya, M.; Muramatsu, A. Solvothermal Synthesis of SrTiO3 Nanoparticles Precisely Controlled in Surface Crystal Planes and Their Photocatalytic Activity. *Appl. Catal. B Environ.* **2014**, *144*, 462−467.
(44) Yanqing, Z.; Erwei, S.; Zhizhan, C.; Wenjun, L.; Xingfang, H. Influence of Solution Concentration on the Hydrothermal Preparation of Titania Crystallites. *J. Mater. Chem.* **2001**, *11*, 1547−1551.
(45) Woo, S.; Jeong, H.; Lee, S. A.; Seo, H.; Lacotte, M.; David, A.; Kim, H. Y.; Prellier, W.; Kim, Y.; Choi, W. S. Surface Properties of Atomically Flat Poly-Crystalline SrTiO 3. *Sci. Rep.* **2015**, *5*, 8822.
(46) Ma, Y.; Wu, Z.; Wang, H.; Wang, G.; Zhang, Y.; Hu, P.; Li, Y.; Gao, D.; Pu, H.; Wang, B.; Qi, X. Synthesis of Nanocrystalline Strontium Titanate by a Sol-Gel Assisted Solid Phase Method and Its Formation Mechanism and Photocatalytic Activity. *CrystEngComm* **2019**, *21*, 3982−3992.
(47) Zhang, Y.; Xu, G.; Wei, X.; Ren, Z.; Liu, Y.; Shen, G.; Han, G. Hydrothermal Synthesis, Characterization and Formation Mechanism of Self-Assembled Mesoporous SrTiO 3 Spheres Assisted with Na 2SiO 3·9H 2O. *CrystEngComm* **2012**, *14*, 3702−3707.
(48) Calderone, V. R.; Testino, A.; Buscaglia, M. T.; Bassoli, M.; Bottino, C.; Viviani, M.; Buscaglia, V.; Nanni, P. Size and Shape Control of SrTiO3 Particles Grown by Epitaxial Self-Assembly. *Chem. Mater.* **2006**, *18*, 1627−1633.
(49) Li, Y.; Xie, X.; Liu, J.; Cai, M.; Rogers, J.; Shen, W. Synthesis of α-Ni(OH)2 with Hydrotalcite-like Structure: Precursor for the Formation of NiO and Ni Nanomaterials with Fibrous Shapes. *Chem. Eng. J.* **2008**, *136*, 398−408.
(50) Tran, P. H.; Thi Hang, A. H. Deep Eutectic Solvent-Catalyzed Arylation of Benzoxazoles with Aromatic Aldehydes. *RSC Adv.* **2018**, *8*, 11127−11133.
(51) Liu, H.; Zhang, B.; Shi, H.; Tang, Y.; Jiao, K.; Fu, X. Hydrothermal Synthesis of Monodisperse Ag2Se Nanoparticles in the Presence of PVP and KI and Their Application as Oligonucleotide Labels. *J. Mater. Chem.* **2008**, *18*, 2573−2580.
(52) Pan, X.; Chen, X.; Yi, Z. Photocatalytic Oxidation of Methane over SrCO3 Decorated SrTiO3 Nanocatalysts via a Synergistic Effect. *Phys. Chem. Chem. Phys.* **2016**, *18*, 31400−31409.
(53) Lavinscky, A. B. S.; Welsch, A. M.; Kennedy, B. J.; Bernardi, M. I. B.; Mastelaro, V. R. Order-Disorder Phenomena and Octahedral Tilting in SrTi 1-X Sn X O 3 Perovskites − A Structural and Spectroscopic Study. *J. Solid State Chem.* **2019**, *269*, 521−531.
(54) Arnal, P.; Corriu, R. J. P.; Leclercq, D.; Mutin, P. H.; Vioux, A. A Solution Chemistry Study of Nonhydrolytic Sol-Gel Routes to Titania. *Chem. Mater.* **1997**, *9*, 694−698.
(55) Luan, W.; Gao, L. Influence of PH Value on Properties of Nanocrystalline BaTiO3 Powder. *Ceram. Int.* **2001**, *27*, 645−648.
(56) Voorhees, P. W. The Theory of Ostwald Ripening. *J. Stat. Phys.* **1985**, *38*, 231−252.
(57) Plimpton, S. Fast Parallel Algorithms for Short-Range Molecular Dynamics. *J. Comput. Phys.* **1995**, *117*, 1−19.
(58) Dong, L.; Luo, Q.; Cheng, K.; Shi, H.; Wang, Q.; Weng, W.; Han, W. Q. Facet-Specific Assembly of Proteins on SrTiO3 Polyhedral Nanocrystals. *Sci. Rep.* **2014**, *4*, 5084.
(59) Balankura, T.; Qi, X.; Fichthorn, K. A. Solvent Effects on Molecular Adsorption on Ag Surfaces: Polyvinylpyrrolidone Oligomers. *J. Phys. Chem. C* **2018**, *122*, 14566−14573.
(60) Vanommeslaeghe, K.; Hatcher, E.; Acharya, C.; Kundu, S.; Zhong, S.; Shim, J.; Darian, E.; Guvench, O.; Lopes, P.; Vorobyov, I.; Mackerell, A. D., Jr. CHARMM General Force Field: A Force Field for Drug-like Molecules Compatible with the CHARMM All-Atom Additive Biological Force Fields. *J. Comput. Chem.* **2009**, *31*, 671−690.
(61) Zhou, Y.; Saidi, W. A.; Fichthorn, K. A. A Force Field for Describing the Polyvinylpyrrolidone-Mediated Solution-Phase Synthesis of Shape-Selective Ag Nanoparticles. *J. Phys. Chem. C* **2014**, *118*, 3366−3374.

https://dx.doi.org/10.1021/acsomega.0c04343
ACS Omega 2020, 5, 33007−33016